Front. Optoelectron. China 2011, 4(1): 93–102
DOI 10.1007/s12200-011-0211-4

RESEARCH ARTICLE

Quantum dot photoelectrochemical solar cells based on TiO_2-$SrTiO_3$ heterostructure nanotube array scaffolds

Jun ZHANG (✉)[1], Chengchun TANG[2]

1 Wuhan National Laboratory for Optoelectronics (WNLO) and College of Optoelectronic Science and Engineering, Huazhong University of Science and Technology, Wuhan 430074, China
2 School of Material Science and Engineering, Hebei University of Technology, Tianjin 300130, China

Abstract Titania-Strontium titanate (TiO_2-$SrTiO_3$) nanotube array with heterostructure has been demonstrated as an efficient scaffold applied to quantum dot photoelectrochemical solar cells. Quantum dot CdS serviced as solar light absorbent is chosen as an example to illustrate superior performance and deposited on scaffolds by successive ionic layer adsorption and reaction (SILAR) technique. The photoelectrochemical performance of such solar cell is strongly dependent on the structure of heterostructured scaffolds. Only well-dispersed $SrTiO_3$ nanocrystallites on TiO_2 could improve the overall conversion efficiency. Transient absorption spectra and photoelectrochemical measurements show that the formation of $SrTiO_3$ energy gradient between TiO_2 and electrolyte slows down the rate of electronic injection from 19.3×10^8 to 6.30×10^8 s^{-1}, while it greatly increases electronic collection efficiency via reduced charge recombination. Cadmium sulfide (CdS) quantum dots used to decorate TiO_2-$SrTiO_3$ (1 h hydrothermal treatment) electrode exhibits superior photoelectrochemical performance with nearly 70% increase in external quantum efficiency at 460 nm and also in overall cell conversion efficiency. The photostability and high efficiency properties of TiO_2-$SrTiO_3$ composites would enable its practical application in solar energy conversion devices.

Keywords quantum dot, heterostructure, nanotube array, photoelectrochemistry, TiO_2

1 Introduction

Semiconductor nanocrystals or quantum dots (QDs) have attracted significant attention of researchers in recent years due to their unique features for the development of next generation solar cells [1]. The substitution of quantum dots to dye to sensitize the oxide film scaffolds is often perceived to take the advantages of quantum dots, such as, greater photostability compared to organometallic or even pure organic dyes, and the ability to modulate the photoresponse in the visible light spectrum by size quantization [2–6]. In addition, the performance of quantum dot based devices can further be boosted by the creation of hot electron and/or multiple exciton generation through high energy excitation [7–10]. By utilizing such hot photogenerated carriers, the solar cells of quantum dot have the potential to obtain considerable conversion efficiency of attainable thermodynamic solar photon, the maximum is up to 66% at one sun intensity [2]. However, in spite of these potential advantages, the solar efficiency of liquid junction of quantum dot photoelectrochemical solar cells (QDSC) has reached only below 5% sensitized by CdSe and CdS together at present [11–14], while dye based solar cells have maximum one above 11%.

In general, photocurrent density (J_{sc}) can be approximately expressed by the following equation:

$$J_{sc} = q\eta_{1abs}\eta_{1nj}\eta_{cc}I_0, \quad (1)$$

where q is elementary charge, η_{labs} is the efficiency of light absorption of a cell, η_{inj} is charge-injection efficiency from quantum dots to oxide scaffolds, η_{cc} is charge-collection efficiency and I_0 is incident photon flux. η_{labs} is determined by optical absorption properties and the amount of adsorbed quantum dots. Many researchers have explored different approaches to modify mesoporous metal oxide films with various quantum dots, such as CdS (Cadmium sulfide) [15,16], CdSe (Cadmium selenide) [17–20], InP (Indium phosphide) [21], InAs (Indium arsenide) [4], and PbS (Lead sulfide) [22], which show the high absorption of light in the visible light region. One major factor that contributes to the lower solar conversion efficiency of

Received October 18, 2010; accepted December 30, 2010

E-mail: jzhangnano@mail.hust.edu.cn

QDSCs than dye-sensitized solar cells (DSSCs) is the surface states (charge traps) on the absorbing semiconductor quantum dots, which offer more potential pathways for recombination in the QDSCs. Such recombination could be greatly suppressed either by coating the quantum dots with a suitable band-aligned semiconductor shell and/or by adsorbing long chain organic passivating molecules [13]. It has been demonstrated that the driving force of charge injection from CdSe quantum dot into TiO_2 could be modulated by varying the particle size of CdSe due to the shift in the conduction band [17]. The difference of energetic level in conduction band between the quantum dots and oxide scaffolds determine the charge injection efficiency; the more negative potential of quantum dots than oxide films in conduction band, the higher charge injection rate.

η_{cc} is largely determined by the competition between charge recombination and transportation in oxide films. For fast transportation, one common strategy that has been extensively studied is the use of single-crystal, wide band gap semiconductor one-dimensional architectures as the electron transport materials since the pioneering work by Yang [16,18,19,23–28]. Such structures facilitate transport of charge carriers with greater efficiency than mesoscopics or particulate semiconductor films by avoiding the particle-to-particle hopping thus minimize the loss of charge carries at grain boundaries. To minimize the recombination of charge carries, an energy gradient that directs the electrons toward the substrate has been introduced between the light sensitizers and oxide films, which prevents back-injection of electrons in the oxide into dye and/or nanocrystals. Such approach involves composite material electrodes in which the two materials differ by their conduction band potential. In addition to suppressing recombination, the foreign material raises cell open-circuit potential directly with more negative conduction band edge than the oxide film or shifts the band edge of the oxide upward in energy if it creates a dipole at the interface [29–31]. This stragety has been extensively investigated especially in DSSCs with many systems [32–35].

However, few attention has been taken on strategy by employing both of above mentioned concepts to facilitate charge carries transportation and minimize recombination simultaneously since such attractive core-shell nanowire structures have been employed in DSSCs [36,37]. Recently, TiO_2 nanotubes with a ZnO (Zinc oxide) thin energy gradient has been used in quantum dot solar cells for improved charge-collecting efficiency and reduced recombination [38]. It should be noted that the introduced ZnO film is subjected to photo-corrosion in aqueous electrolyte with the UV light irradiation [39]. Only few inorganic materials, such as TiO_2, $SrTiO_3$, and SnO_2 (Tin oxide) are stable enough to be used as practical solar energy conversion devices,which do not subject to decomposition upon irradiation when used as photoelectrodes in aqueous media [40]. Based on the consideration for possible practical application, we have developed a hydrothermal method to obtain TiO_2-$SrTiO_3$ heterostructure nanotube array electrodes with tunable morphology, composition and phtoelectrochemical properties (Scheme 1) [41]. Well dispersed $SrTiO_3$ nanocrystallites on TiO_2 nanotube arrays could improve the overall photoelectrochemical performance due to the charge separation within the heterostructures. We speculated that such heterostructures should have excellent ability as the scaffolds for light absorbent in photoelectrochemical solar cells, which has been preliminarily investigated in our recent communication [42]. In this article, we will give systemic results on such TiO_2-$SrTiO_3$ heterostructure arrays with different structure as conducting scaffolds in a photoelectrochemical solar cell, in which CdS quantum dot chosen as a demonstration is deposited by a traditional chemical precipitation technique referred to as an successive ionic layer adsorption and reaction (SILAR) [15,16,42,43] (Scheme 1). By combining the properties of exciton generation in CdS quantum dots, the facilitated charge capture and transport characteristics of TiO_2 nanotube arrays also with the reduced charge recombina-

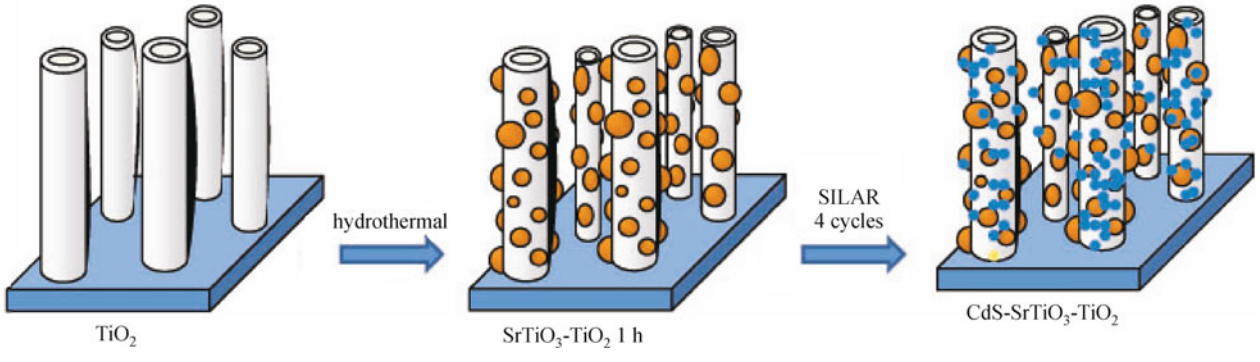

Scheme 1 Illustration to synthesis of TiO_2-$SrTiO_3$ heterostructure nanotube arrays and deposite CdS quantum dots on the surface by SILAR technique

tion process by energy gradient, we have succeeded in developing an effective strategy for harvesting solar energy through CdS-TiO_2-$SrTiO_3$ composites. Photochemical processes that follow the excitation of CdS QDs, as probed by transient absorption and photoelectrochemical measurements, are presented.

2 Experiments

2.1 CdS quantum dots deposition by SILAR method

The detailed fabrication process of TiO_2 nanotubes and corresponding TiO_2-$SrTiO_3$ heterostructure nanotube arrays could be found in our recent publication [41]. Briefly, TiO_2 nanotube ordered arrays are produced by electrochemical etching of Ti electrodes in fluoride media on the Ti strips. Upon annealing in air, these arrays form anatase crystallites while maintaining the tubular morphology. TiO_2-$SrTiO_3$ heterostructure nanotube arrays were prepared by hydrothermal method utilizing the formed anatase films as a TiO_2 source as well as a structure-directing scaffold. By varying the hydrothermal reaction times, the amount of $SrTiO_3$ coating was readily tuned. The prepared TiO_2 and TiO_2-$SrTiO_3$ (1 h and 2 h) nanotube array electrodes were successively exposed to $CdSO_4$ (Cadmium sulfate) and Na_2S (Sodium sulfide) solutions to deposit CdS quantum dots. To keep the deposition procedure identical, the three electrodes were simultaneously immersed in a solution of $CdSO_4$ (0.1 M) for four minutes. Then, they were taken out to rinse with deionized water separately. After drying, they were immersed in a Na_2S (0.1 M) solution for another four minutes together, followed by another rinsing with deionized water and drying. This constituted one cycle. This SILAR process was repeated until the desired deposition of CdS nanocrystallites was achieved.

2.2 Characterization of electrodes

The composition and crystal structure of the obtained films were examined by an X-ray diffractometer (XRD, Scintag X1 advanced diffraction system). A field-emission scanning electron microscope (Hitachi S-4800 FESEM) was used to observe the morphologies of the electrodes. Diffuse reflectance absorption spectra were recorded using a Shimadzu UV-3101PC spectrophotometer; Ti (Titanium) foil preheated at 450°C under air was used as a reference. Ultrafast femtosecond transient absorption spectroscopy was conducted using a Clark-MXR 2010 laser system and an optical detection system provided by Ultrafast Systems (Helios). TiO_2 and TiO_2-$SrTiO_3$ nanotube arrays were detached from the substrates by sonication in methanol for 1 h. They were spin coated onto optically transparent electrodes (OTE), and then following by depositing with CdS QDs by SILAR. Prior to experiment, the samples were vacuumed for one night. The laser system is capable of delivering 775 nm laser pulses of 1 mJ/pulse with fwhm equal to 150 fs at a rate of 1 kHz. 5% of the output beam was used to generate a probe pulse. The second harmonic (387 nm) was used for excitation of the sample.

2.3 Photoelectrochemical measurements

Photoelectrochemical behavior of electrodes was carried out in a two-armed cell with a Pt-gauze counter-electrode, aqueous 0.1 M Na_2S solution as a redox couple. Photocurrent measurements and *I-V* characteristics were carried out using a Keithley 2601 sourcemeter along with collimated, filtered light ($\lambda > 400$ nm, 100 mW/cm^2) from an Oriel 300 W xenon lamp. For incident photon to charge carrier generation efficiency (IPCE) measurements, a Bausch and Lomb high-intensity grating monochromator was introduced into the path to select an excitation wavelength.

3 Results and discussion

Electrochemical anodization of Ti metal is a relatively simple approach for the fabrication of TiO_2 nanotube arrays, which has been extensively investigated by Grimes and Schmuki's groups to alter the morphological properties, such as their pore diameter, wall thickness, intertube spacing, and tube length and so on [28,44,45]. The fascinating nanotube arrays could be used as the structure-directing template for the fabrication of other materials, which is similar to carbon nanotubes template. In addition, it is also capable of servicing as the Ti source to produce titanate nanotubes or TiO_2-titanate heterostructures. Our recent investigation shows that the crystallinity of TiO_2 precursor determinates the structure of final products during hydrothermal treatment. Pure $SrTiO_3$ nanotubes could be obtained using amorphous TiO_2 nanotube arrays as Ti source and template. In contrast, TiO_2-$SrTiO_3$ heterostructures could be fabricated from anatase nanotube arrays, in which the amount of $SrTiO_3$ coating was readily tuned by varying the duration of hydrothermal reaction. The typical SEM images of anatase, TiO_2-$SrTiO_3$ with 1 h and 2 h reaction time are shown in Fig. 1. Separated nanoparticles of $SrTiO_3$ with a diameter of about 50 nm were formed on the surface of TiO_2 nanotubes when anatase nanotubes were subjected to 1 h hydrothermal treatment, while uniform nanoparticle films were formed after 2 h or longer reaction time (Fig. 1(c)).

3.1 Surface modification with CdS QDs

Generally, two methods are commonly used for the assembly of QDs on electrodes. The first is the in situ synthesis of QDs in the substrate using SILAR or chemical bath deposition (CBD) technique [15]. The another is the

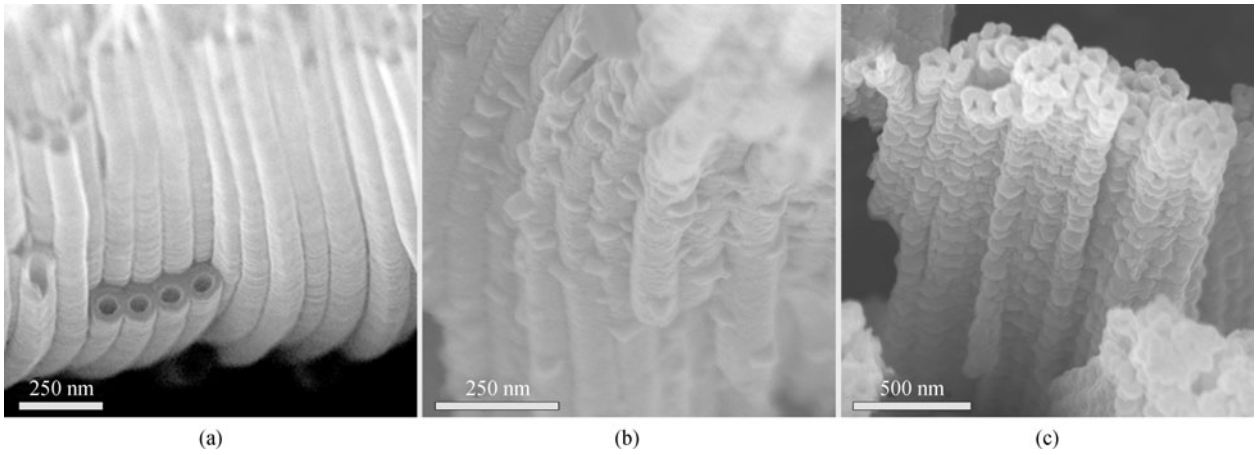

Fig. 1 SEM images of different scaffolds. (a) Anatase TiO_2 nanotube arrays by electrochemical anodization; and TiO_2-$SrTiO_3$ heterostructure nanotube arrays after hydrothermal treatment with (b) 1h and (c) 2h (Ref. [42], published with permission)

self-assembled binding of the prepared QDs to TiO_2 surface through the linking of a bifunctional molecule [3]. Due to the simplicity and feasibility of SILAR technique, CdS QDs are effectively deposited on TiO_2-$SrTiO_3$ heterostructure nanotube array scaffolds for solar cell application. The significant visual color change could be observed after CdS deposition shown in the photograph of Fig. 2, which identifies the formation of CdS nanocrystalities on the substrate. The formation of QDs with size quantization effect is evidenced from the absorption spectra in Fig. 3, in which the absorption edge shifts directly to red with successive deposition cycles. To compare the influence of different scaffolds to anchor light harvests in the performance of solar cells, all of the samples in the following discussion are deposited with 4 cycles. The XRD spectra (Fig. 4) of TiO_2 and TiO_2-$SrTiO_3$ heterostructures before and after modification with CdS also identify the formation of CdS by the adopted SILAR method. The peaks corresponding to CdS are broad as shown by the circle and reflect the small size of CdS nanocrystallites, which is consistent with our claim for the formation of quantum dots.

Fig. 2 Photographs of TiO_2-$SrTiO_3$ (1h) nanotube array electrodes before (upper) and after (below) CdS deposition

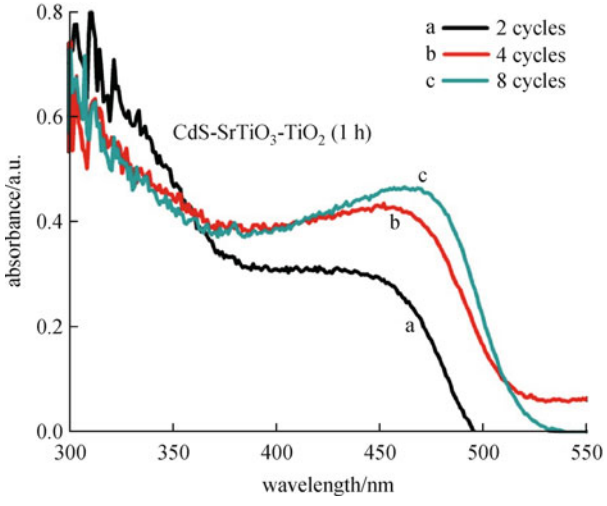

Fig. 3 Diffuse reflectance absorption spectra of TiO_2-$SrTiO_3$ electrodes following different cycle's deposition of CdS quantum dots

3.2 Transient absorption studies

Transient absorption spectrophotoscopy is a useful instrument to evaluate or measure the electron transfer rate from one semiconductor to another one. To compare the influence of scaffolds on the bleaching recovery of CdS QDs, electrode with pristine CdS quantum dots formed on SiO_2 colloid film on OTE substrate were used as a reference. It has been shown that metal chalcogenide quantum dots undergo anodic corrosion in the presence of air when exposed to light due to leaving behind reactive holes [19]. To minimize the photodecomposition during laser excitation process for transient absorption measurements, the samples were vacuumed overnight prior to experiment. The transient absorption spectra were recorded at different delay times following the 387 nm laser pulse

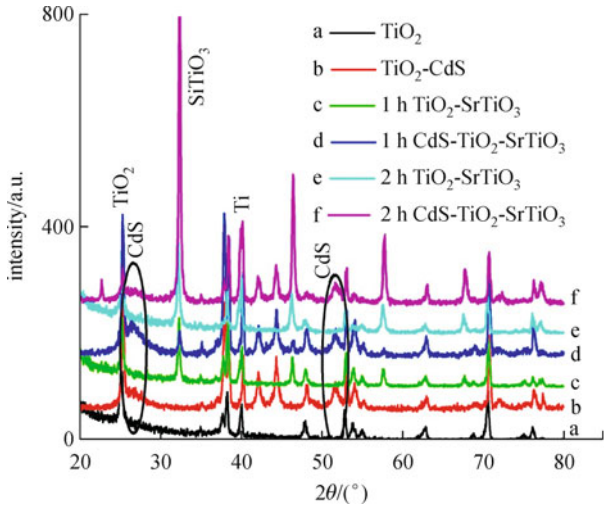

Fig. 4 XRD patterns of TiO_2 and TiO_2-$SrTiO_3$ heterostructure nanotube arrays with different hydrothermal duration before and after CdS modification

excitation. Figures 5 (a)–5(c) show the transient absorption spectra of CdS-SiO_2, CdS-TiO_2, and CdS-TiO_2-$SrTiO_3$ (1 h), respectively. It is evident that all of the three samples have a bleaching in the 450–550 nm regions. Generally, the bleaching recovery process with increasing time is determinated from the separated charge carriers disappear rate either via recombination or by electron transfer to oxide scaffolds (Eqs. (2) and (3)). The analysis of transient bleaching recovery is usually used to elucidate the kinetics of the charge injection process. The recovery of the transient bleaching was multiexponential and was analyzed using biexponential fits (Eq. (4)) shown in Fig. 5(d), in which to compare the bleaching recovery of the three films at bleaching maximum wavelength. Fitted values are tabulated in Table 1.

$$\mathrm{CdS} + h\nu \rightarrow \mathrm{CdS}(\mathrm{e}^- + \mathrm{h}^+) \rightarrow \mathrm{CdS} \tag{2}$$

$$\mathrm{CdS}(\mathrm{e}^- + \mathrm{h}^+) + \mathrm{TiO_2/SrTiO_3} \rightarrow \mathrm{CdS}(\mathrm{h}^+) + \mathrm{TiO_2/SrTiO_3}(\mathrm{e}^-) \tag{3}$$

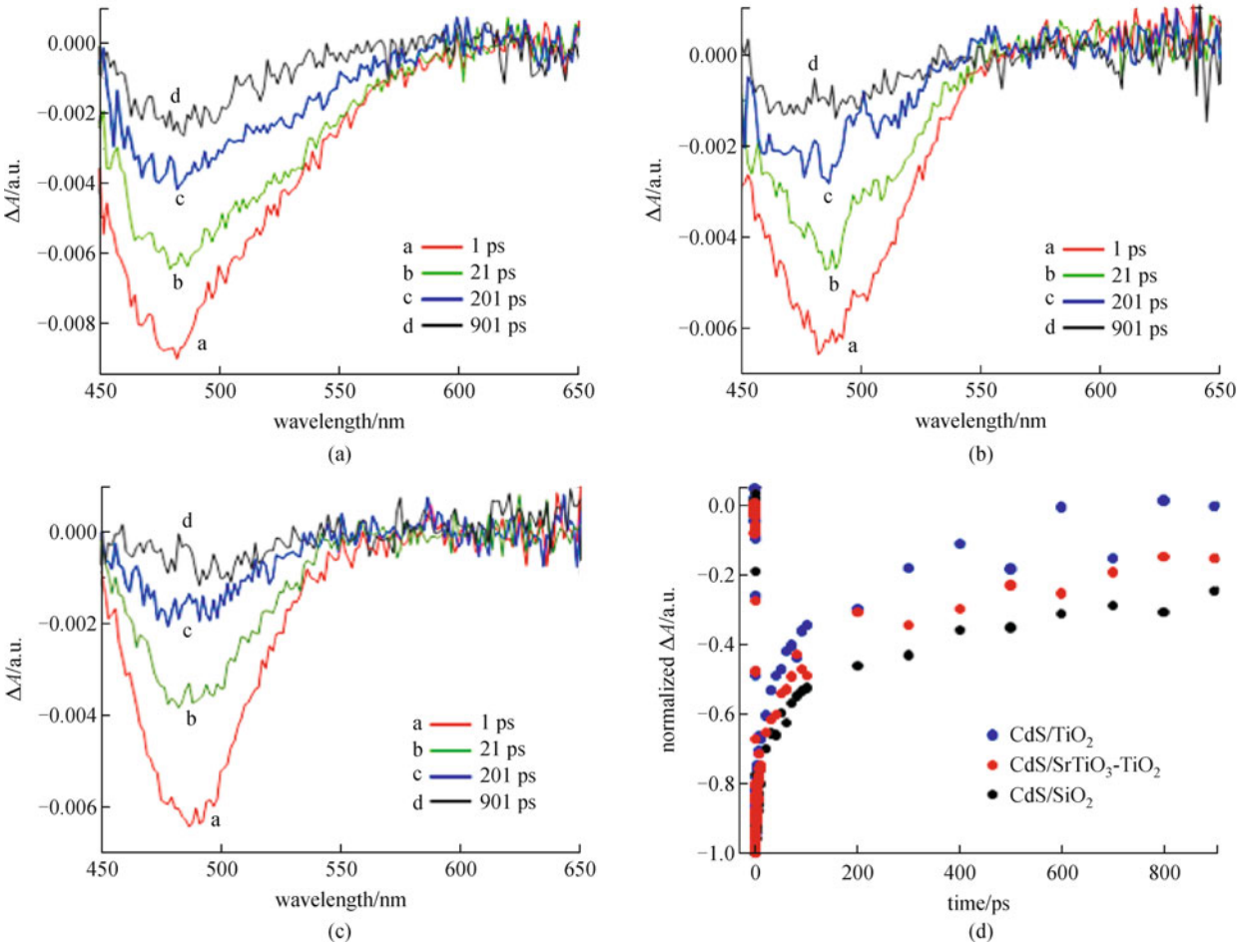

Fig. 5 Time-resolved transient absorption spectra of (a) film of CdS quantum dots on SiO_2 colloid film on OTE; (b) TiO_2 and (c) TiO_2-$SrTiO_3$ nanotube films coated with CdS on OTE; (d) the bleaching recovery normalized to peak response (Ref. [42], published with permission)

Table 1 Fitted kinetic parameters of the time-resolved transient absorption bleaching recovery for CdS-SiO_2, CdS-TiO_2, and CdS-TiO_2-$SrTiO_3$ films on OTE

	y_0	a_1	τ_1/ps	a_2	τ_2/ps	‹τ›/ps
CdS-SiO_2	−0.15	−0.479	561.48	−0.358	13.42	551.86
CdS-TiO_2	0	−0.574	271.022	−0.427	6.032	266.71
CdS-TiO_2-$SrTiO_3$	−0.08	−0.516	416.158	−0.374	9.505	409.54

$$y = y_0 + a_1^{-t/\tau_1} + a_2^{-t/\tau_2} \tag{4}$$

For comparison purposes, the average lifetimes were determined using Eq. (5) [46].

$$\langle\tau\rangle = \frac{a_1\tau_1^2 + a_2\tau_2^2}{a_1\tau_1 + a_1\tau 1}. \tag{5}$$

Based on the fitted biexponential values, we observe that the bleaching recovery in the TiO_2 and TiO_2-$SrTiO_3$ supported CdS is faster than CdS-SiO_2 system. CdS-SiO_2, CdS-TiO_2, and CdS-TiO_2-$SrTiO_3$ films have long-lived bleaching recovery with average lifetimes of 551.86, 266.71, and 409.54 ps, respectively. The faster recovery in the CdS-TiO_2/TiO_2-$SrTiO_3$ arises as the electron transfer from CdS to TiO_2 or $SrTiO_3$, which dominates the deactivation of CdS QDs. It should be noted that the bleaching recovery is slow down by the introduction of $SrTiO_3$ nanoparticles on the TiO_2 surface compared to CdS-TiO_2 film.

We estimated the electron transfer rate constant from CdS by comparing the bleaching recovery lifetimes in the presence and absence of scaffolds. If the dominant pathway responsible for the faster bleaching recovery of CdS on scaffold surface is assumed to ascribe to electron transfer, the transfer rate could be estimated using Eq. (6).

$$k_{et} = 1/\tau_1 - 1/\tau_0, \tag{6}$$

where τ_1 and τ_0 represent the average lifetime of bleaching recovery in the presence and absence of scaffolds, respectively. Based on the analysis, we observe a decrease in the electron transfer rate constant from 19.3×10^8 to 6.30×10^8 s^{-1} as we introduced $SrTiO_3$ nanoparticles onto the surface of TiO_2. It means TiO_2-$SrTiO_3$ heterostructure nanotube array scaffold does not favor the electron transfer from light-harvesting assemblies. This result is consistent with our previous observation that coupling $SrTiO_3$ nanoparticles shifts the Fermi level of composite to more negative potentials, causing the decrease of driving force for charge injection and correspondingly slowing down electron injection rate.

3.3 Photoelectrochemistry

The transient absorption studies indicate that $SrTiO_3$ nanoparticles coupled on TiO_2 retard the electron injection from excited CdS QDs. However, they are quite effective in minimizing the charge recombination from conduction band of scaffolds to oxidized sensitizer and/or redox couple in electrolyte, as will be discussed in the following sections. The absorption properties of visible light of CdS QDs, as well as the ability to capture and transport electrons into substrate of the TiO_2-$SrTiO_3$ scaffolds, pave the way for their applications in photoelectrochemical solar cells. We compared the photoelectrochemcial behavior of CdS coupled TiO_2 nanotube arrays in the presence and absence of $SrTiO_3$ coaters. Two-armed cell was applied for the evaluation the photoelectrochemical performances with Pt as a counter electrode and aqueous 0.1 M Na_2S as the electrolyte. Upon visible light illumination, we observed a prompt photocurrent in both CdS-TiO_2 and CdS-TiO_2-$SrTiO_3$ (1 h) cases (Figs. 6(a) and 6(b)). It is obvious that the CdS-TiO_2-$SrTiO_3$ electrode exhibits superior performance with greater photocurrent generation efficiency than that of CdS-TiO_2. The photocurrent response to repeated on-off cycles of visible light illumination shows the stability and reproducibility of the observed photocurrent in these systems. In addition, we also present the photocurrent of CdS coupled TiO_2-$SrTiO_3$ heterostructures via 2 h hydrothermal reaction. Significant low photocurrent was observed (Fig. 6(c)). It may be ascribed to the electron transport in the independent $SrTiO_3$ coater limited by their grain boundaries rather than through TiO_2 nanotubes [41].

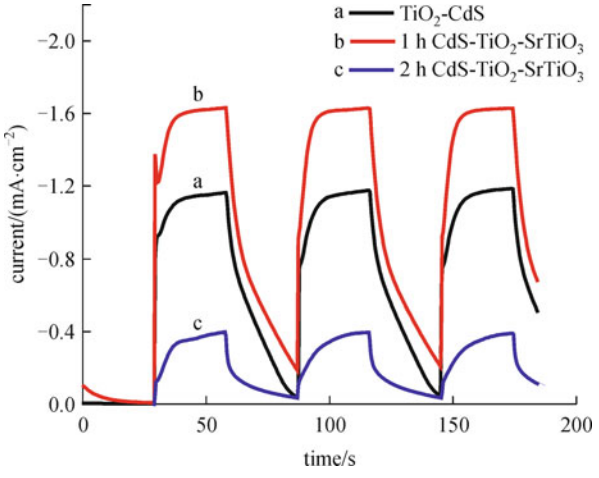

Fig. 6 Current versus time measurements of electrodes of (a) CdS-TiO_2, and CdS deposited TiO_2-$SrTiO_3$ heterostructure nanotube arrays with (b) 1h and (c) 2h hyderothermal duration

Shown in Fig. 7 are photocurrent density-voltage (*J-V*) characteristic curves of both QDSCs based on different photoanodes. The performance parameters of the QDSCs are listed in Table 2. It has been known that the open circuit potential of quantum dot solar cells is greater than that of corresponding dye sensitized or polymer hybrid solar cells [15]. However, the power conversion efficiency obtained

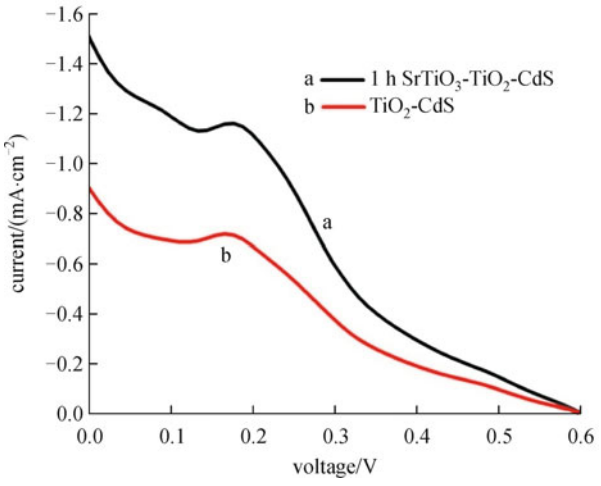

Fig. 7 *J-V* characteristic curves of QDSCs based on TiO_2 nanotube and $SrTiO_3$-TiO_2 heterostructures, respectively

Table 2 Cell performance parameters of QDSCs based on two electrodes, corresponding to *J-V* characteristic curves in Fig. 7

electrode	V_{oc} /V	J_{sc} /(mA·cm^{-2})	fill factor (*FF*) /%	effiency /%
CdS-TiO_2	0.611	0.9	25.45	0.14
$SrTiO_3$-TiO_2-CdS	0.611	1.54	24.44	0.23

with CdS-TiO_2-$SrTiO_3$ (1 h) system still remained quite low due to the presence of charge traps on the absorbing semiconductor surface [13]. Therefore, it is possible to achieve higher power conversion efficiency by adopting our synthesized TiO_2-$SrTiO_3$ heterostructure nanotube array scaffolds coupled with both CdS and CdSe QDs. Efforts are underway to couple TiO_2-$SrTiO_3$ (1 h) with multi- short bandgap semiconductors to harvest photons in the whole spectrum region of the solar light to boost overall cell efficiency.

Incident photon to charge carries generation efficiency (IPCE) was monitored to compare the photoresponse of both electrodes (CdS sensitized TiO_2 nanotube array scaffolds with and without $SrTiO_3$ nanoparticles coating) to monochromatic light irradiation using Eq. (7).

$$\mathrm{IPCE}(\%) = [1240/\lambda(\mathrm{nm})][I_{sc}(\mathrm{A/cm^2})/P_i(\mathrm{W/cm^2})] \times 100. \quad (7)$$

P_i is the power of monochromatic light of wavelength λ (nm) incident on the electrode, and I_{sc} is short-circuiting current. The IPCE spectra for CdS-TiO_2 and CdS-TiO_2-$SrTiO_3$ electrodes are shown in Fig. 8 (a). Both electrodes show similar response with a photocurrent onset just below 500 nm. Also, the photoresponse of every electrode matches well with the corresponding absorption spectra in Fig. 8(b), which confirms the origin of the photocurrent generation to be the excitation of CdS. The maximum IPCE value of the CdS-TiO_2-$SrTiO_3$ (1 h) was 35.4% as compared to 20.5% IPCE of alone TiO_2 nanotube scaffold. The higher efficiency observed for CdS-TiO_2-$SrTiO_3$ electrode suggests the superior performance for the introduction of $SrTiO_3$ nanoparticles on TiO_2 surface as scaffold for solar cells. It is interesting to note that the maximum optical absorption value of CdS-TiO2 is higher than that of CdS-TiO_2-$SrTiO_3$ electrode. Qualitative analysis on the efficiency of charge recombination between two electrodes was conducted using Eq. (8) [19].

$$\mathrm{IPCE} = \eta_{1abs}\eta_{inj}\eta_{cc}. \quad (8)$$

The CdS-TiO_2 electrode possesses higher light absorption efficiency (Fig. 8(b)) and faster electron injection rate

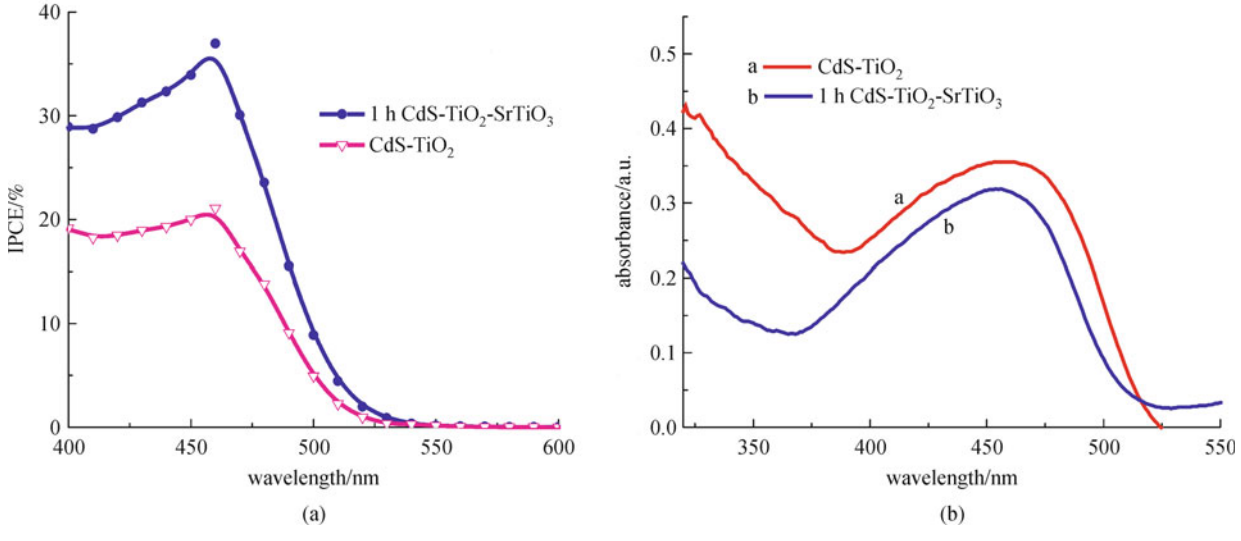

Fig. 8 (a) IPCE and (b) diffuse reflectance UV-vis absorption spectra of CdS quantum dots deposited TiO_2 and TiO_2-$SrTiO_3$ heterostructure nanotube array electrodes

from CdS to TiO_2 scaffold, while has lower IPCE value. It could be deduced that the charge collection efficiency of TiO_2-$SrTiO_3$ scaffolds should be greatly higher than that of TiO_2 alone. Caution should be taken that dry electrodes were used to compare the η_{labs} and η_{inj}, under conditions different from those to which a solar cells exposed. Observed from the SEM image of TiO_2-$SrTiO_3$ (1 h) (Fig. 1), $SrTiO_3$ nanoparticles are separately dispersed on TiO_2 naotube surface. The electron transport process of TiO_2-$SrTiO_3$ into substrate should be similar to that of TiO_2 along aligned nanotube arrays. Thus, charge transportation values on both electrodes are assumed to be same. Therefore, the charge recombination is greatly reduced by the introduction of energy gradient of $SrTiO_3$.

We further assessed the photoelectrochemical behavior by monitoring the cell potential response to on-off cycles of visible light illumination (Fig. 9(a)). An open circuit potential (V_{oc}) of 630±20 mV was observed for both cases following excitation with visible light. It indicates that no significant change occurs for the Fermi level of TiO_2 after depositing $SrTiO_3$ nanoparticles, which is consist with our previous observation that 50 mV negative shift in Fermi level for TiO_2-$SrTiO_3$ heterostructures. However, the V_{oc} decay upon turning off the light does not share the same trend, which is generally used to investigate the recombination kinetics of electrodes. It represents the removal of electrons in charge recombination and/or charge transfer across the semiconductor interface into redox couple injection. The electron lifetime is determined by the open circuit potential decay using the following expression:

$$\tau_n = \frac{-Tk_B}{e}\left[\frac{dV_{OC}}{dt}\right]^{-1}. \quad (9)$$

Figure 9(b) is the plot of the electron lifetime obtained by applying Eq. (9) to the data in Fig. 9(a). The CdS-TiO_2-$SrTiO_3$ electrode exhibit superior recombination characteristics, with the longer lifetimes indicating fewer charge recombinations, confirming the better performance of producing higher photocurrents compared to CdS-TiO_2 nanotube arrays.

An energy-level illustration for the possible transfer of electrons from CdS to scaffolds through the electrolyte is schematically presented in Fig. 10. The energetic alignment between CdS and TiO_2 favors the electron injection from excited CdS into TiO_2. The electrons captured by the TiO_2 nanotube arrays are quickly transported through the vertical nanotube direction toward the substrate surface. Electron injected into scaffolds is subject to two possible recombination processes: recombination with the oxidized sensitizer and/or with redox couple in the electrolyte. It is expected that in the presence of $SrTiO_3$ nanoparticles between TiO_2 and electrolyte, such two possible recombination processes of photoinjected electrons would be suppressed as the higher conduction energy level of $SrTiO_3$ than that of TiO_2. Not only can $SrTiO_3$ build cascaded band alignment, but it can also passivate the surface traps. In addition, the discontinuous distribution of $SrTiO_3$ nanoparticles on TiO_2 surface ensure the electron trans-

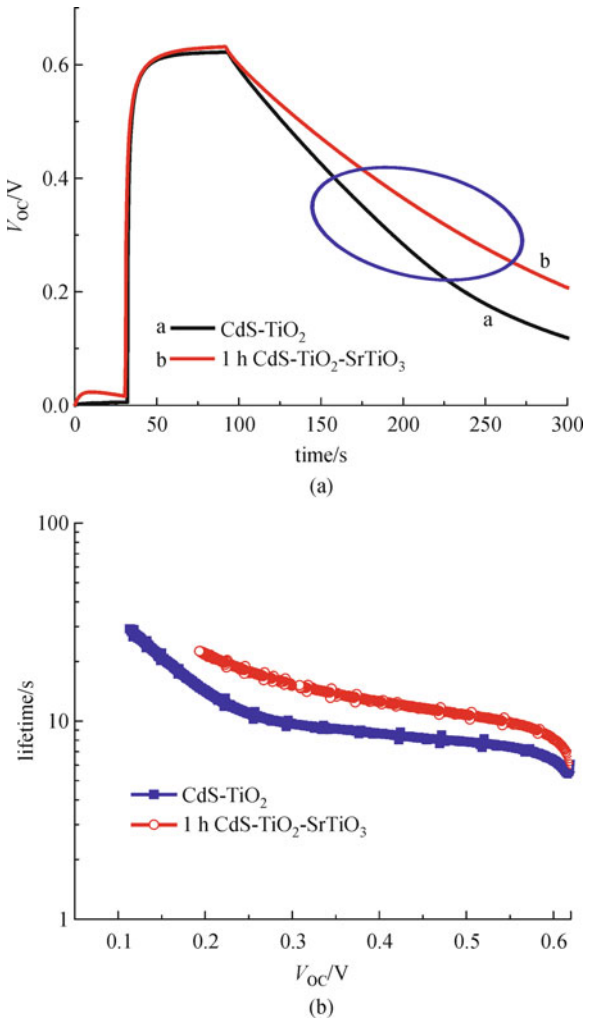

Fig. 9 (a) Open circuit potential response to on-off visible light illumination and (b) electron lifetimes versus open circuit potential of CdS-TiO_2 and CdS-TiO_2-$SrTiO_3$ electrodes

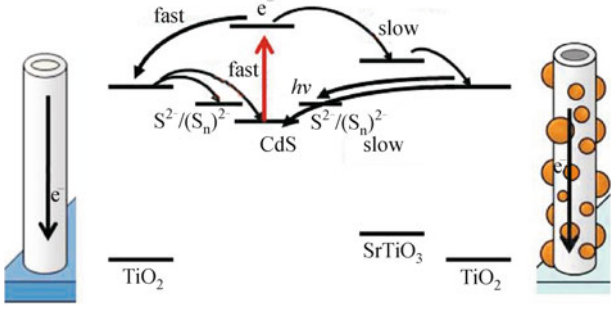

Fig. 10 Schematic energy diagram of CdS quantum dot sensitized TiO_2 nanotube arrays in the absence and precence of $SrTiO_3$ nanoparticle coating

portation through vertical TiO_2 nanotube arrays, which takes the advantage of one-dimensional structures for electron transportation compared to mesoscopics or particulate semiconductor films. Based on the short circuit photocurrent, IPCE and V_{oc} decay measurements, we can conclude that TiO_2 nanotube array with $SrTiO_3$ nanoparticles coating serves as high efficiency scaffold architecture to facilitate capture and collection of electrons from CdS QDs.

4 Conclusions

Transient absorption spectra and photoelectrochemical performance of CdS QDs sensitized solar cells made using TiO_2 nanotube array scaffold in the absence and presence of $SrTiO_3$ nanoparticles on surface were compared. Despite a slower electron injection rate, TiO_2-$SrTiO_3$ heterostructure nanotube arrays with 1h hydrothermal reaction were shown to improve performances of QDs solar cells by the introduction of energy gradient of $SrTiO_3$ to reduce the charge recombination. Altogether, the novel TiO_2-$SrTiO_3$ heterostructre system provides a promising direction toward developing effective light energy conversion devices, especially in quantum dot photoelectrochemical solar cells.

Acknowledgements This work was supported by the China Scholarship Council for the research grant. We gratefully acknowledge Dr. J H Bang, and Prof. P V Kamat for helpful discussion.

References

1. Kamat P V. Quantum dot solar cells. semiconductor nanocrystals as light harvesters. Journal of Physical Chemistry C, 2008, 112(48): 18737–18753
2. Nozik A. Quantum dot solar cells. Journal of Physics of the Earth, 2002, 14(1–2): 115–120
3. Robel I, Subramanian V, Kuno M, Kamat P V. Quantum dot solar cells. harvesting light energy with CdSe nanocrystals molecularly linked to mesoscopic TiO_2 films. Journal of the American Chemical Society, 2006, 128(7): 2385–2393
4. Yu P, Zhu K, Norman A G, Ferrere S, Frank A J, Nozik A J. Nanocrystalline TiO_2 solar cells sensitized with InAs quantum dots. J Phys Chem B, 2006, 110(50): 25451–25454
5. Luther J M, Law M, Beard M C, Song Q, Reese M O, Ellingson R J, Nozik A J. Schottky solar cells based on colloidal nanocrystal films. Nano Letters, 2008, 8(10): 3488–3492
6. Weiss E A, Porter V J, Chiechi R C, Geyer S M, Bell D C, Bawendi M G, Whitesides G M. The use of size-selective excitation to study photocurrent through junctions containing single-size and multi-size arrays of colloidal CdSe quantum dots. Journal of the American Chemical Society, 2008, 130(1): 83–92
7. Ross R T, Nozik A J. Efficiency of hot-carrier solar energy converters. Journal of Applied Physics, 1982, 53(5): 3813–3818
8. Schaller R D, Klimov V I. High efficiency carrier multiplication in PbSe nanocrystals: implications for solar energy conversion. Physical Review Letters, 2004, 92(18): 186601
9. Schaller R D, Agranovich V M, Klimov V C. High-efficiency carrier multiplication through direct photogeneration of multi-excitons via virtual single-exciton states. Nature Physics, 2005, 1(3): 189–194
10. Luther J M, Beard M C, Song Q, Law M, Ellingson R J, Nozik A J. Multiple exciton generation in films of electronically coupled PbSe quantum dots. Nano Letters, 2007, 7(6): 1779–1784
11. Niitsoo O, Sarkar S K, Pejoux C, Ruhle S, Cahen D, Hodes G J. Chemical bath deposited CdS/CdSe-sensitized porous TiO_2 solar cells. Photochemistry and Photobiology A, 2006, 181(2–3): 306–313
12. Diguna L J, Shen Q, Kobayashi J, Toyoda T. High efficiency of CdSe quantum-dot-sensitized TiO_2 inverse opal solar cells. Applied Physics Letters, 2007, 91(2): 023116
13. Hodes G. Comparison of dye- and semiconductor-sensitized porous nanocrystalline liquid junction solar cells. Journal of Physical Chemistry C, 2008, 112(46): 17778–17787
14. Lee Y L, Lo Y S. Highly efficient quantum-dot-sensitized solar cell based on Co-sensitization of CdS/CdSe. Advanced Functional Materials, 2009, 19(4): 604–609
15. Baker D R, Kamat P V. Photosensitization of TiO_2 nanostructures with CdS quantum dots. particulate versus tubular support architectures. Advanced Functional Materials, 2009, 19(5): 805–811
16. Sun W T, Yu Y, Pan H Y, Gao X F, Chen Q, Peng L M. CdS quantum dots sensitized TiO_2 nanotube-array photoelectrodes. Journal of the American Chemical Society, 2008, 130(4): 1124–1125
17. Robel I, Kuno M, Kamat P V. Size-dependent electron injection from excited CdSe quantum dots into TiO_2 nanoparticles. Journal of the American Chemical Society, 2007, 129(14): 4136–4137
18. Kongkanand A, Tvrdy K, Takechi K, Kuno M K, Kamat P V. Quantum dot solar cells. Tuning photoresponse through size and shape control of CdSe-TiO_2 architecture. Journal of the American Chemical Society, 2008, 130(12): 4007–4015
19. Leschkies K S, Divakar R, Basu J, Enache-Pommer E, Boercker J E, Carter C B, Kortshagen U R, Norris D J, Aydil E S. Photosensitization of ZnO nanowires with CdSe quantum dots for photovoltaic devices. Nano Letters, 2007, 7(6): 1793–1798
20. Lee H J, Yum J H, Leventis H C, Zakeeruddin S M, Haque S A, Chen P, Seok S I, Gratzel M, Nazeeruddin M K. CdSe Quantum dot-sensitized solar cells exceeding efficiency 1% at full-sun Intensity. Journal of Physical Chemistry C, 2008, 112(30): 11600–11608
21. Zaban A, Micic O I, Gregg B A, Nozik A J. Photosensitization of nanoporous TiO_2 electrodes with InP quantum dots. Langmuir, 1998, 14(12): 3153–3156
22. Plass R, Pelet S, Krueger J, Gratzel M, Bach U. Quantum dot sensitization of organic-inorganic hybrid solar cells. Journal of Physical Chemistry B, 2002, 106(31): 7578–7580
23. Law M, Greene L E, Johnson J C, Saykally R, Yang P. Nanowire dye-sensitized solar cells. Nature Materials, 2005, 4(6): 455–459
24. Martinson A B F, Elam J W, Hupp J T, Pellin M J. ZnO nanotube based dye-sensitized solar cells. Nano Letters, 2007, 7(8): 2183–2187
25. Mor G K, Shankar K, Paulose M, Varghese O K, Grimes C A. Use of

highly-ordered TiO_2 nanotube arrays in dye-sensitized solar cells. Nano Letters, 2006, 6(2): 215–218

26. Zhu K, Neale N R, Miedaner A, Frank A J. Enhanced charge-collection efficiencies and light scattering in dye-sensitized solar cells using oriented TiO_2 nanotubes arrays. Nano Letters, 2007, 7 (1): 69–74
27. Jennings J R, Ghicov A, Peter L M, Schmuki P, Walker A B. Dye-sensitized solar cells based on oriented TiO_2 nanotube arrays: transport, trapping, and transfer of electrons. Journal of the American Chemical Society, 2008, 130(40): 13364–13372
28. Shankar K, Basham J I, Allam N K, Varghese O K, Mor G K, Feng X, Paulose M, Seabold J A, Choi K S, Grimes C A. Recent Advances in the Use of TiO_2 Nanotube and Nanowire Arrays for Oxidative Photoelectrochemistry. Journal of Physical Chemistry C, 2009, 113(16): 6327–6359
29. Diamant Y, Chen S G, Melamed O, Zaban A. Core-shell nanoporous electrode for dye sensitized solar cells:the effect of the $SrTiO_3$ shell on the electronic properties of the TiO2 core. Journal of Physical Chemistry B, 2003, 107(9): 1977–1981
30. Diamant Y, Chappel S, Chen S G, Melamed O, Zaban A. Core-shell nanoporous electrode for dye sensitized solar cells: the effect of shell characteristics on the electronic properties of the electrode. Coordination Chemistry Reviews, 2004, 248(13–14): 1271–1276
31. Bandaranayake K M P, Indika-Senevirathna M K, Prasad-Weligamuwa P M G M, Tennakone K. Dye-sensitized solar cells made from nanocrystalline TiO_2 films coated with outer layers of different oxide materials. Coordination Chemistry Reviews, 2004, 248(13–14): 1277–1281
32. Nasr C, Kamat P V, Hotchandani S.. Photoelectrochemistry of composite semiconductor thin films. II. Photosensitization of SnO_2/ TiO_2 coupled system with a ruthenium polypyridyl complex. Journal of Physical Chemistry B, 1998, 102(49): 10047–10056
33. Zaban A, Chen S G, Chappel S, Gregg B A. Bilayer nanoporous electrodes for dye sensitized solar cells. Chemical Communications, 2000, 14(22): 2231–2232
34. Wang Z S, Huang C H, Huang Y Y, Hou Y J, Xie P H, Zhang B W, Cheng H M. A highly efficient solar cell made from a dye-modified ZnO-covered TiO_2 nanoporous electrode. Chemistry of Materials, 2001, 13(2): 678–682
35. Palomares E, Clifford J N, Haque S A, Lutz T, Durrant J R. Control of charge recombination dynamics in dye sensitized solar cells by the use of conformally deposited metal oxide blocking layers. Journal of the American Chemical Society, 2003, 125(2): 475–482
36. Law M, Greene L E, Radenovic A, Kuykendall T, Liphardt J, Yang P. ZnO-A_2O_3 and ZnO-TiO_2 core-hell nanowire dye-sensitized solar cells. Journal of Physical Chemistry B, 2006, 110(45): 22652–22663
37. Kang S H, Kim J Y, Kim Y, Kim H S, Sung Y E. Surface modification of stretched TiO_2 nanotubes for solid-state dye-sensitized solar cells. Journal of Physical Chemistry C, 2007, 111 (26): 9614–9623
38. Lee W, Kang S H, Kim J Y, Kolekar G B, Sung Y E, Han S H. TiO_2 nanotubes with a ZnO thin energy barrier for improved current efficiency of CdSe quantum-dot-sensitized solar cells. Nanotechnology, 2009, 20(33): 335706
39. Zhang L, Cheng H, Zong R, Zhu Y. Photocorrosion suppression of ZnO nanoparticles via hybridization with graphite-like carbon and enhanced photocatalytic activity. Journal of Physical Chemistry C, 2009, 113(6): 2368–2374
40. Fujihira M, Ohishi N, Osa T. Photocell using covalently-bound dyes on semiconductor surfaces. Nature, 1977, 268(5617): 226–228
41. Zhang J, Bang J H, Tang C, Kamat P V. Tailored TiO_2-$SrTiO_3$ heterostructure nanotube arrays for improved photoelectrochemical performance. ACS Nano, 2010, 4(1): 387–395
42. Zhang J, Tang C, Bang J H. CdS/TiO_2-$SrTiO_3$ heterostructure nanotube arrays for improved solar energy conversion efficiency. Electrochemistry Communications, 2010, 12(8): 1124–1128
43. Nicolau Y F. Solution deposition of thin solid compound films by a successive ionic-layer adsorption and reaction process. Applications of Surface Science, 1985, 22–23(2): 1061–1074
44. Likodimos V, Stergiopoulos T, Falaras P, Kunze J, Schmuki P. Phase composition, size, orientation, and antenna effects of self-assembled anodized titania nanotube arrays: a polarized micro-raman investigation. Journal of Physical Chemistry C, 2008, 112 (33): 12687–12696
45. Macák J M, Tsuchiya H, Schmuki P. High-aspect-ratio TiO_2 nanotubes by anodization of titanium. Angewandte Chemie International Edition, 2005, 44(14): 2100–2102
46. James D R, Liu Y S, de Mayo P, Ware W R. Distributions of fluorescence lifetimes: consequences for the photophysics of molecules adsorbed on surfaces. Chemical Physics Letters, 1985, 120(4–5): 460–465